RANDOM SEQUENTIAL ADSORPTION OF SHAPES WITH RANDOM GEOMETRY: THE CASE OF RECTANGLES WITH RANDOM ASPECT RATIO*

Luca Petrone

via B. Cesana 6, 20132 Milano, Italy

Received 1 February 2022, accepted 27 April 2022, published online 19 May 2022

In a previous paper, we studied Random Sequential Adsorption of rectangles with the constant area but random aspect ratio. Here, we investigate the statistical distribution of the density at saturation, the hyperuniformity of the packing, and revisit the analysis of the Available Surface Function and Feder's law. We also evaluate the performance of the algorithm used in the simulations.

DOI:10.5506/APhysPolB.53.5-A1

1. Introduction

Random Sequential Adsorption (RSA) is a numerical protocol that generates random packings with a very simple rule: it randomly selects position and orientation of a virtual particle and, if there is no intersection with any of the other particles already present, it is added to the packing, and its position will remain fixed for all the rest of the process — for this reason the term Adsorption was given by Feder [1], who noticed that such two-dimensional packings resemble the structure of monolayers obtained in irreversible adsorption experiments.

Most of the RSA studies are focused on packings built of mono-disperse objects of the same shape and many different geometries have been considered, through the years. In 2D, for example, they range from the classic geometries (disks [2], squares [3], polygons [4], and ellipses [5]), to more exotic shapes such as smoothed dimers [6], discorectangles [7], star polygons [8], and polygons with rounded corners [9].

Much less attention was paid to mixtures [10, 11] and polydisperse particles. About the latter, in Ref. [12], the effect of uniform and Gauss distribution of spherical particle diameter on jamming coverage and kinetics

* Presented at the XXXIV Marian Smoluchowski Symposium on Statistical Physics, 27–29 September, 2021.

parameters was analyzed. In Refs. [13, 14], a continuum power-law size distribution $P(R) \sim R^{(\alpha-1)}$ with $R \in (0, R_{\max}]$ for disk radii was considered, instead: this implies that the estimation of the density at saturation is meaningless, since in the limit of infinite time, the whole space will be ultimately filled with particles and the density will be trivially equal to 1, but in such patterns, a fractal nature is revealed and order is emerging while α is increasing. In fact, this is closely related with the Apollonian packing — the first discovered fractal — which is the limit of this kind of packing for $\alpha \to \infty$.

Nevertheless, before our study in Ref. [15], there were no other approaches to RSA packings built of particles with random geometry, but fixed area. Being the size of the deposited particles always non-vanishing, the value of density at saturation can never reach 1 and, therefore, is worth to be evaluated. The easiest way to add randomness to a shape is to consider rectangles with a fixed area and variable aspect ratio[1]. The results of such a study were presented in Ref. [15].

In this paper, we start from this study and we want to investigate the influence of finite simulation time on the packing fraction estimation [16] that was not included in the original paper. We also want to revise the fitting of the Available Surface Function, which was not satisfactory. Finally, we add some evaluation of the algorithm and its performance.

2. Simulation description

At each iteration, a random point inside a square of side length L is selected. Then another value, randomly taken from the interval $(1/L, 1)$[2], is used to define the ratio between the two sides of the rectangle with a unit area. Finally, the orientation of the rectangle (horizontal or vertical) is also chosen randomly. Now, the process can proceed according to the above-mentioned RSA protocol [1, 17]: if the rectangle with the unitary area defined as above does not overlap any particle already placed in the packing, it is added, otherwise, it is rejected. These steps are repeated until there is no space to place any other particle: at this stage, the packing is saturated.

Periodic boundary conditions are used to decrease finite-size effects [18].

[1] The core of the algorithm is the geometrical construction of virtual rectangular cells, surrounded by deposited particles. Since the sides of these cells must be in common with the sides of the deposited particles, the latter can be neither curved, nor oriented in the space. For this reason, only oriented rectangles can benefit from that algorithm.

[2] The limit for low values of the aspect ratio is required in order to avoid having rectangles with one side longer than the packing side L.

3. Algorithm

The approaching of the RSA packing density to the jamming limit θ_{sat} after n depositions is usually governed by a relation of the kind (see Section 4.3)

$$\theta_{\text{sat}} - \theta(n) = A\, n^{-1/d} \tag{3.1}$$

with A and d constant. Based on this fact, the convergence to the limit is generally very slow. Therefore, some strategies must inevitably be followed in order to speed up the calculation and reach the saturation in a reasonable time.

The first step is to implement a grid, covering the whole packing, in order to perform the check of intersection of the virtual particle with the other rectangles only for good candidates. For this purpose, for each cell of the grid, we generate a list of rectangles that have some overlap with it and keep it updated at each iteration.

A further step would be to decrease the size of the grid and remove the cells which are completely overlapped by rectangles in order to reduce the surface over which the deposition is allowed. However, due to the peculiar geometry of this RSA, most of the particles are elongated rectangles, which are not thick enough to fully overlap a cell and, consequently, remove it from the list. Additionally, an excluded zone around each rectangle cannot be uniquely defined because the minimum distance between it and the nearest neighbour is not fixed, but depends on the aspect ratio of the neighbour itself. For this reason, it is not possible to have the formation of "clusters" of overlapping excluded areas, with the consequent removal of cells fully covered by them and, therefore, no grid mesh refining is performed.

The last and most effective strategic step is to identify the areas, located between the deposited rectangles, that are suitable to accommodate new particles. For each of them, only the small central portion is considered available for deposition, and this significantly increases the efficiency of the algorithm.

Due to the high effectiveness, especially of the last step, it is easy to simulate fully saturated RSA configurations, with the dimension of the packings comparable with what has been done for other classical geometries. The most important thing, however, is that the results, especially in terms of density at saturation, are exact and not an extrapolation-based over runs performed halting the generation after some arbitrary number of unsuccessful tries of adding new objects to the packing. In fact, only for a few RSA geometries [2, 4, 9, 19], efficient algorithms have been developed in order to obtain strictly saturated configurations.

Full details of the algorithm used can be found in Ref. [15].

4. Analysis of the results

An example of packing is shown in Fig. 1.

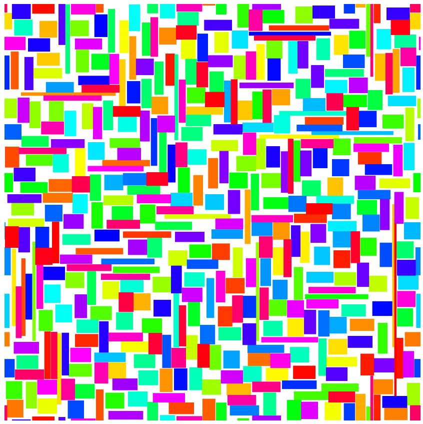

Fig. 1. Example RSA packing built of aligned rectangles of unit area and uniformly distributed random aspect ratio.

4.1. Mean saturated packing fraction

The main parameter describing an RSA packing is the mean saturated packing fraction θ_{sat}, which is the ratio of the area covered by N particles of area $S_{\mathrm{p}} = 1$ to the area of the whole packing $S = L^2$

$$\theta_{\mathrm{sat}} = \left\langle \frac{NS_{\mathrm{p}}}{S} \right\rangle = \left\langle \frac{N}{S} \right\rangle , \tag{4.1}$$

where $\langle\cdot\rangle$ denotes averaging over a set of independent random packings. The average is well defined and the packing fraction is normally distributed (see Fig. 2)

Simulations have been performed for several different values of L between 100 and 1000, with at least 100 runs for each size, in order to exclude the presence of any effect due to the finite size of the packing. The data depicted in Fig. 3 do not show any systematic dependence on packing size, thus we consider the density at saturation θ_{sat} to be equal to 0.678689 ± 0.000019, which is the average value obtained from 130 independent, saturated packings of a side length size $L = 1000$ — the largest dimension analysed.

4.2. Shape distribution influence on packing fraction

In Ref. [15], we showed that the distribution of parameter f, describing the rectangle shape (aspect ratio), changes during the RSA process: at the

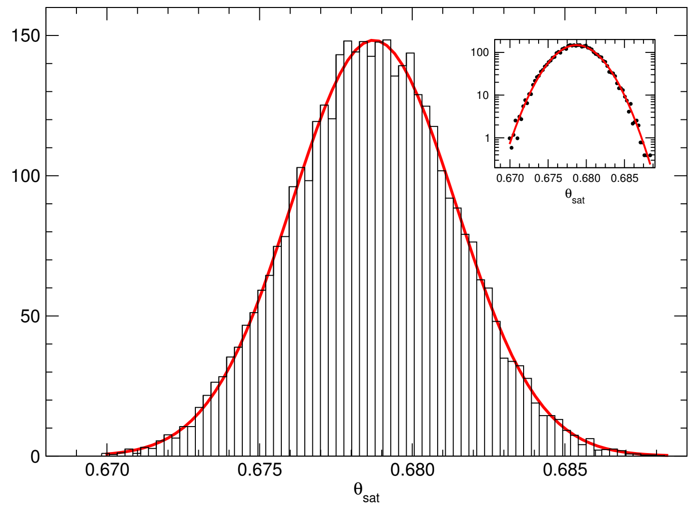

Fig. 2. Histogram of saturated packing fractions obtained from 20 000 independent packings with $L = 125$. The red line corresponds to a normal distribution of an average 0.67848 and a standard deviation 0.00269. Inset shows the same plot in a log–normal scale. The histogram was normalized to represent probability distribution.

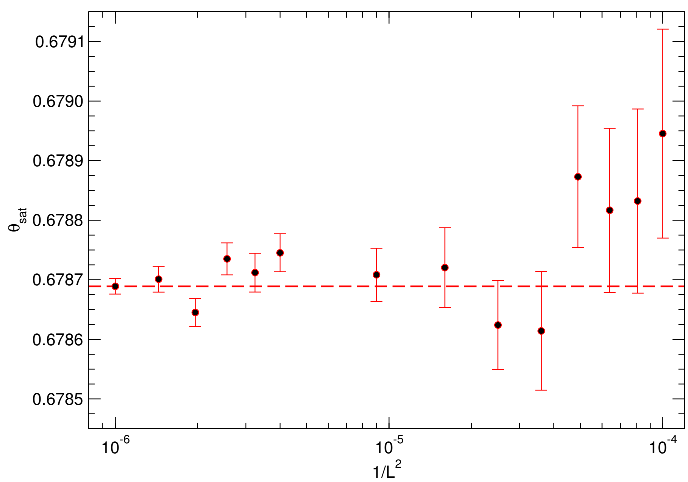

Fig. 3. The mean saturated packing fraction as a function of the inverse of packing surface size $S = L^2$, with bars denoting the Standard Error of the Means. The red dashed line corresponds to $\theta_{\mathrm{sat}} = 0.678689$.

beginning, when the coverage is low, it is almost uniform and reflects the distribution of the random variable used for its sampling, but, with the increase of the coverage, the number of highly anisotropic rectangles decreases, and then, when the density reaches about the 75% of the value at saturation, there is an increase of rectangles of low to moderate anisotropy, while rectangles with higher aspect ratios start to disappear. When rectangles start to interact with each other, due to the increase of density, interstices begin to appear: this implies that both very elongated shapes and rectangles similar to squares cannot find enough free space — they are deposited mainly at the beginning of packing generation when they do not find any obstacles.

The change of the shape distribution during packing generation, as a consequence of the evolution of the inner geometry of the packing itself, suggests that the packing fraction may change if the probability distribution used to select the side length ratios of the rectangles is varied. In order to evaluate this effect, in Ref. [15] we considered a more general function, as done by Brilliantov for Polydisperse RSA [13, 14]

$$p_f(x) = (\alpha + 1)x^{\alpha} \tag{4.2}$$

with $\alpha \in (-1, +\infty)$. For high positive values of α, square-like shapes are more probable, while negative values of α favour anisotropic shapes. The mean packing fraction dependence on α is shown in Fig. 4. Figure 5 shows the patterns of the packing for $\alpha \to -1$ and $\alpha \to \infty$. The packing fraction grows with the parameter α, but packings with high values of α are very

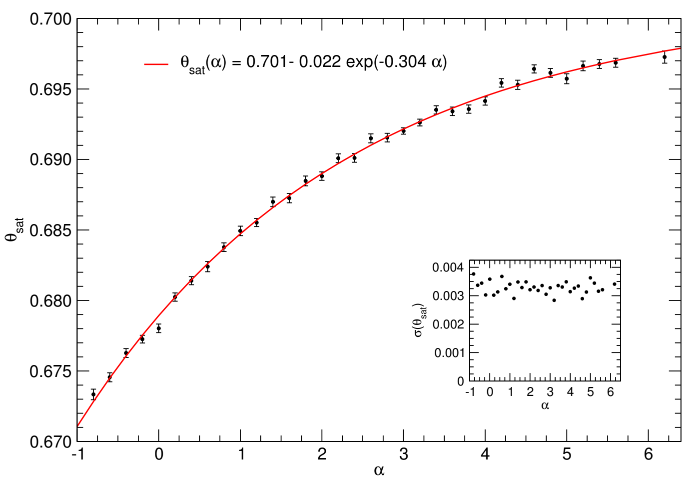

Fig. 4. The mean saturated packing fraction for different α, measured for packing size $L = 50$. Black dots are simulation data and the red solid line is the fitting $\theta_{\mathrm{sat}}(\alpha) = \theta_\infty - A\exp(-k\,\alpha)$. Compare the coefficient $\theta_\infty = 0.701$ with the estimated value of $\theta_{\mathrm{sat}}(\alpha \to \infty) = 0.705902$ calculated for $L = 50$ according to the procedure described in the text. In the inset plot, the standard deviation of θ_{sat} shows no dependency on α.

hard to be obtained. In Section 4.2, we showed that near-saturation shapes of high anisotropies are mainly deposited, thus, in order to reach saturation, we would need to try rectangles with small aspect ratio, but their probability to be chosen rapidly decreases with growing α. Therefore, in this case, the generation of even small saturated packings ($L = 50$) requires a very large amount of time (see Fig. 20 (b)).

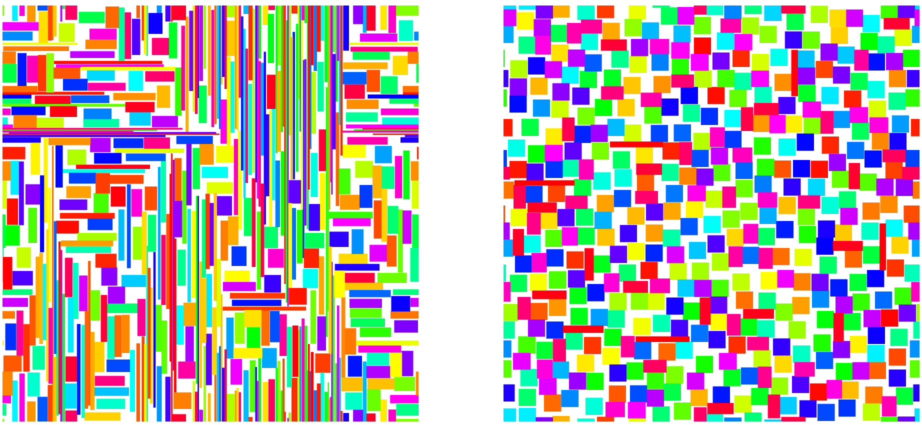

(a) (b)

Fig. 5. Packing for different values of distribution exponent (a) $\alpha \to -1$ (b) $\alpha \to \infty$ showing the different patterns of the two extremals.

Even if we are not able to extend the plot of Fig. 4, is it easy to estimate the packing density in the limit of $\alpha \to \infty$, taking inspiration from what has been described for Polydisperse RSA [14]. In fact, an infinite α means that at each iteration, the selected aspect ratio is always the highest possible. Based on this consideration, the first step of the algorithm is to deposit only squares (which are the rectangles with the highest aspect ratio), until the RSA jamming limit for squares is reached ($\theta \approx 0.562$). Then, at each iteration, the algorithm identifies the position where the rectangle with the largest aspect ratio can be placed, and such a rectangle is deposited, tangent to its neighbours, as shown in Fig. 6 (a), and so on, until the jamming is finally reached. Figure 7 shows how f decreases during the RSA. This is a quasi-deterministic[3] process, quite similar to what happens, for circles, with the Apollonian Packing. From this, we can estimate $\theta_{\mathrm{sat}}(\alpha \to \infty)$.

A higher value of the parameter α means that anisotropic shapes have a lower probability to be selected. If such shapes were deposited in the first stages of the process, they would represent a hindrance to the deposition of the next rectangles, as the latter are forced to have their longer side in the

[3] Actually, even if the dimensions are fixed and the rectangle is tangent to a couple of neighbours in a deterministic way, its position is still free to be chosen randomly.

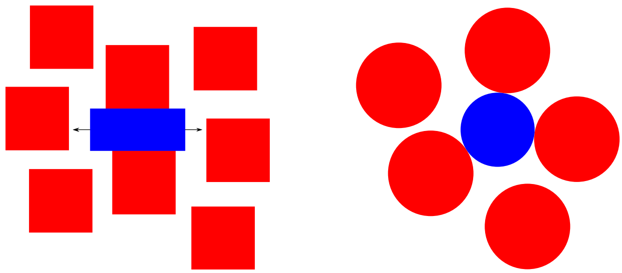

Fig. 6. Placing the rectangle with the highest aspect ratio in order to estimate the packing fraction in the limit of $\alpha \to \infty$ (a). Its position is free to be randomly chosen in the direction parallel to the longest side shown by the arrows — this does not happen for disks with a variable radius (b), since the largest circle that can be deposited is tangent to the others, each one in a single point, and its position has no randomness.

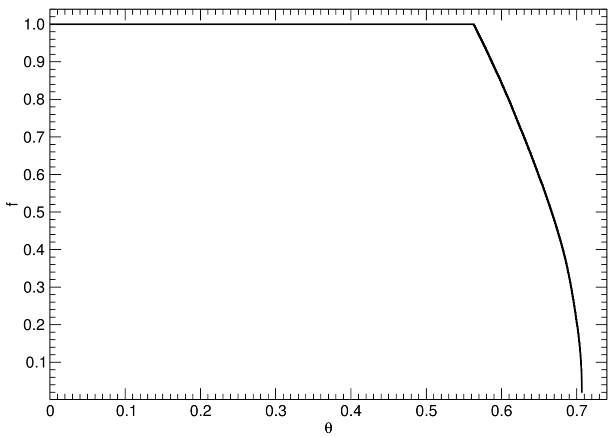

Fig. 7. The aspect ratio f of the rectangle deposited for $\alpha \to \infty$ as a function of density θ.

same direction as those already deposited (see Fig. 8). If, on the other side, anisotropic rectangles are deposited only in the later stages, when most of the rectangles with higher aspect ratios are rejected, they find the space in the small interstices between the adjacent rectangles and contribute to having a denser packing. This is the explanation of why the mean saturated packing fraction is increasing with the parameter α, and the concept is even clearer if we consider the limit of $\alpha \to \infty$, and how it is calculated. Starting from the skeleton built by the squares, rectangles of increasing anisotropy are selected to exactly fill the voids, creating, at the same time, the least obstruction to other rectangles, as they have the highest aspect ratio. This means that the maximum packing density has been reached. As done for $\alpha = 0$, simulations

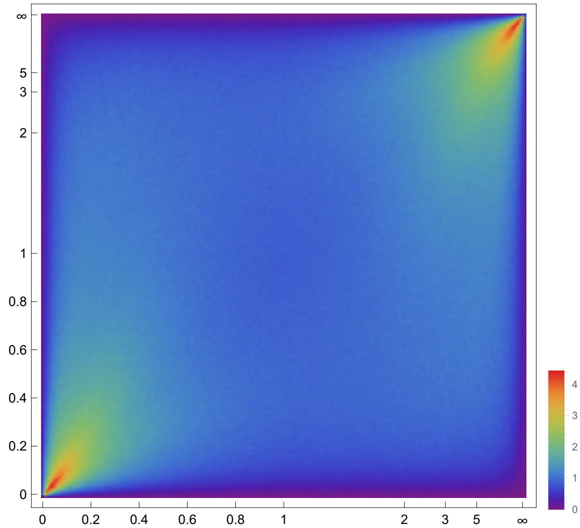

Fig. 8. Probability density for a rectangle with horizontal/vertical side ratio as per x-axis and whose nearest neighbour has a horizontal/vertical side ratio as per y-axis: from this, it emerges that the most probable configuration is an anisotropic shape parallel to others with similar anisotropy.

have been performed for values of L between 100 and 600, with at least 100 runs for each size. In this case, the value of calculated density at saturation is slightly increasing with packing size (see Fig. 9). This behaviour seems to be related to the fact that, with the increase of the packing size, the lowest

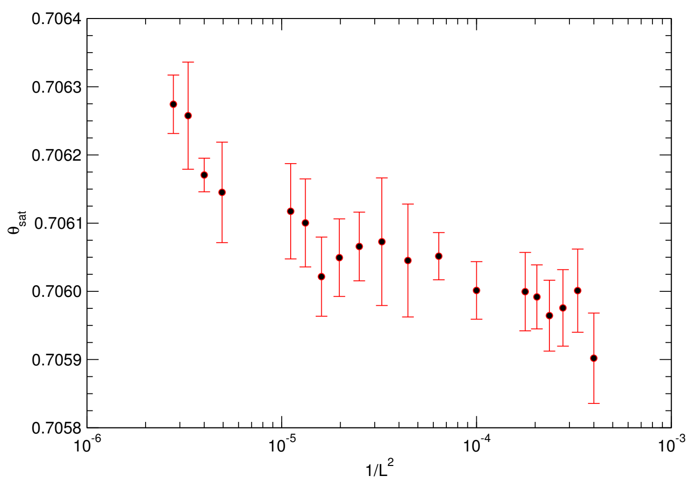

Fig. 9. The mean saturated packing fraction for $\alpha \to \infty$ as a function of the inverse of packing surface size $S = L^2$, with bars denoting the Standard Error of the means.

aspect ratio is decreasing (see Fig. 10). In Ref. [15], we considered the value of density at saturation $\theta_{\rm sat}$ to be equal to 0.706171 ± 0.000025, which was the average value obtained from 200 independent, saturated packings of a side length size $L = 500$ — the largest dimension analysed at that time.

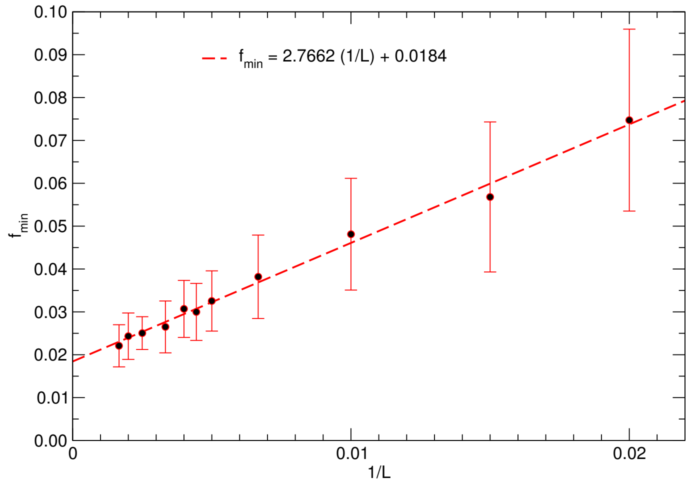

Fig. 10. The lowest aspect ratio (*i.e.* that of the last deposited rectangle) as a function of the inverse of packing size, with bars denoting the Standard Deviation. This suggests that, with larger packing dimensions, more anisotropic particles succeed to find a place to be hosted — and this fact allows to have a slightly higher packing density. Due to the peculiar process with $\alpha \to \infty$, the anisotropic rectangles are deposited after the squares and all the rectangles with lower anisotropy, thus the probability that a very elongated shape finds a free space between the rectangles already deposited is effectively zero (it would be non-zero if the anisotropic rectangles were deposited in the early stages of the process).

Compared with all the other RSAs of shapes with fixed geometry, the packings studied here are significantly denser (Table 1), since the freedom to choose the rectangle shape allows the filling also thin areas, at the later stages of packing generation, that otherwise would not be available for deposition.

4.3. Feder's law

During the generation of random packing, its density increases with subsequent iterations of the RSA procedure, and for systems approaching the jamming limit it is generally governed by the following relation, called Feder's law:

$$\theta_{\rm sat} - \theta(n) = A\, n^{-1/d}\,, \tag{4.3}$$

Table 1. RSA of different shapes and orientations with increasing density at jamming.

Shape	Orientation	Ref.	Anisotropy	Density at saturation
Equilateral Triangles	Random	[4]	1	0.525902(36)
Squares	Random	[4]	1	0.527594(70)
Disks	Fixed	[2]	1	0.5470735(28)
Rectangles	Random	[20]	1.492(22)	0.549632(17)
Squares	Fixed	[3]	1	0.562009(4)
Ellipses	Random	[5]	1.84	0.583999(17)
Rounded Triangles	Random	[21]	—	0.60143(10)
Rectangles with Random Aspect Ratio	Fixed	[15]	—	0.706171(25)

where $\theta(n)$ is the packing density after n RSA iterations[4], θ_{sat} is the packing density at saturation, and A is a positive constant. The parameter d is known to be equal to the packing dimension in the case of disks, balls, and hyper-balls [2, 22, 23], which appeared to be valid also for fractal dimensions [24, 25]. For RSA of unoriented anisotropic shapes in two dimensions, $d = 3$ [26, 27], it was thus conjectured that the parameter d corresponds to the number of degrees of freedom of deposited shapes [28, 29].

For this process, Feder's law is valid. Since saturated packings were generated, we estimated the parameter d using the relation between the median M_n of the number of iterations at which the last particle was added and the packing size L^2 [30]

$$M_n = C\,\left(L^2\right)^{d+1}\,, \tag{4.4}$$

and thus we got $d = 2.94 \pm 0.07$, which is in good agreement with our theoretical expectation of $d = 3$. This method has the advantage to avoid using any interpolation.

The parameter d comes straightforward from (4.3): by manipulation, d can be obtained from the slope of the dependence of $\ln \mathrm{d}\theta(n)/\mathrm{d}n$ on $\ln n$. The main issue is that Feder's law does not specify where the fitting shall be performed. In fact, it models the behaviour of packing for moderate-to-high coverage (the behaviour at low coverage will be studied in Section 4.4), thus

[4] Here, n refers to the number of iterations in the original RSA scheme and not to the steps in our algorithm. If we exclude some regions from random sampling due to the impossibility to place there a new rectangle, and thus, sample only a fraction x of the whole packing surface, then one step in our method statistically corresponds to $1/x$ iterations of the original RSA procedure.

it is crucial to correctly identify the fitting range: if its starting point is too low, the behaviour might not be a power law for the whole range, as the coverage at the lower bound of the range might be not high enough, while if the range is too low, the fitting would be too poor.

Feder's law is also very useful to estimate the density at saturation, as described in Ref. [16]. This information can be taken into consideration for other similar RSAs for which no fully saturated packings can be generated, in order to decide after how many iterations stop the process.

Here, we perform the following:

— for a given $(n, \Delta n)$, we take a range $[n_1, n_2]$, where $n_2 = n_{\rm sat} - n$, $n_1 = n_2 - \Delta n$, $n_{\rm sat}$ is the number of iterations required to fully saturate the packing, and $\Delta n + 1$ is the number of points over which fitting is performed;

— we estimate $\hat{d}$ fitting $\ln \mathrm{d}\theta(n)/\mathrm{d}n$ on $\ln n$ in the range $[n_1, n_2]$;

— using the estimated $\hat{d}$ we evaluate $\hat{\theta}_{\rm sat}$;

— knowing the exact value of $\theta_{\rm sat} = n_{\rm sat}/L^2$, we can calculate the error $\mathrm{d}\theta = |\hat{\theta}_{\rm sat}(n) - \theta_{\rm sat}|$ performed stopping the process n iterations before the saturation.

This process is similar to what has been described in Ref. [16], apart from the fact that in Ref. [16] the interpolation is done in the range of $(0.001n, n)$, which means that the number of points over which the interpolation is performed only depends on n. In fact, for a high n, the number of points included in the range $(0.001n, n)$ could be very low, affecting the estimation of d and θ.

In order to make the analysis independent from the packing dimension, we divide the range extremes by $n_{\rm sat}$. Thus, we actually perform the interpolation between $1 - \phi_1$ and $1 - \phi_2$, where $\phi = n/n_{\rm sat} = \theta(n)/\theta_{\rm sat}$.

First, we perform the interpolation taking $\phi_2 = 1$, and we evaluate $\hat{d}$ and its standard deviation as a function of $\Delta\phi$. As shown in Fig. 11, for low values of $\Delta\phi$ (*i.e.* for a small Δn), the estimation of $\hat{d}$ is affected by a great statistical error, due to the small number of points. Then, the estimated value of d reaches a plateau and remains almost constant until $\Delta\phi \approx 0.015$, where $d = 3.067 \pm 0.044$, which is consistent with the evaluation made above, according to Ref. [30]. For higher values of $\Delta\phi$, $\hat{d}$ starts deviating, which means that the log–log interpolation is no more linear.

Then, we evaluate the mean absolute error $\mathrm{d}\theta$ that we would make on the density, extrapolated according to Ref. [16], if we stop the generation of packing at $\phi < 1$. Plotting the values it emerges that $\mathrm{d}\theta/L$ is independent from the packing size (see Fig. 12)

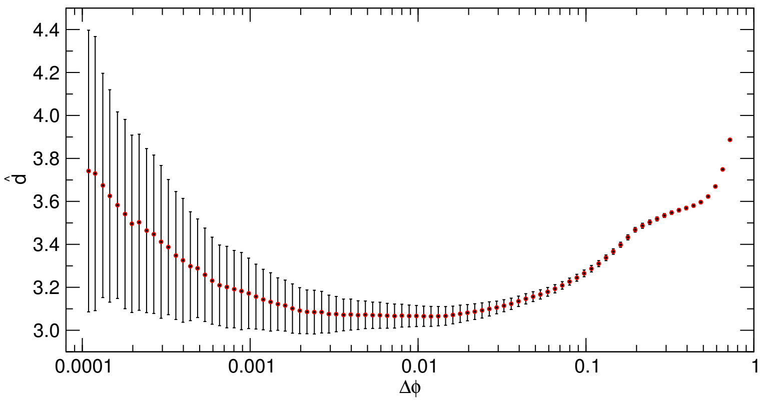

Fig. 11. The estimated value of d for $\alpha = 0$ in the range $(1 - \Delta\phi, 1)$ as a function of $\Delta\phi$, with bars denoting the Standard Deviation.

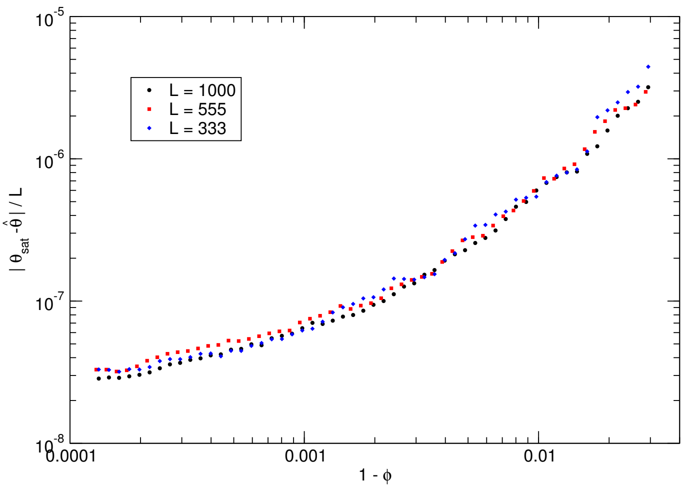

Fig. 12. The estimated value of error dθ divided by the packing size L as a function of the upper bound of the interpolating range (the range width $\Delta\phi$ is taken equal to 0.015), for $L = 333, 555, 1000$.

Therefore, one can use this approach also for an RSA for which fully saturated packings cannot be generated. As described above, the evaluation of d shall be performed as a function of $\Delta\phi$, with the difference that the upper bound of the range is $\phi_{\mathrm{max}} = n_{\mathrm{max}}/n_{\mathrm{sat}}$ instead of 1, where n_{max} is the number of particles after which the process is stopped. Provided Feder's law is applicable for this RSA, the plot of $\hat{d}(\Delta\phi)$ will typically have a plateau. The value of $\Delta\phi$ where the plateau ends will be used to evaluate $\hat{\theta}$ according to Ref. [16]: this will maximize the number of points over which the fitting is performed, while still remaining within a power-law behaviour, giving a better estimation (see Fig. 13).

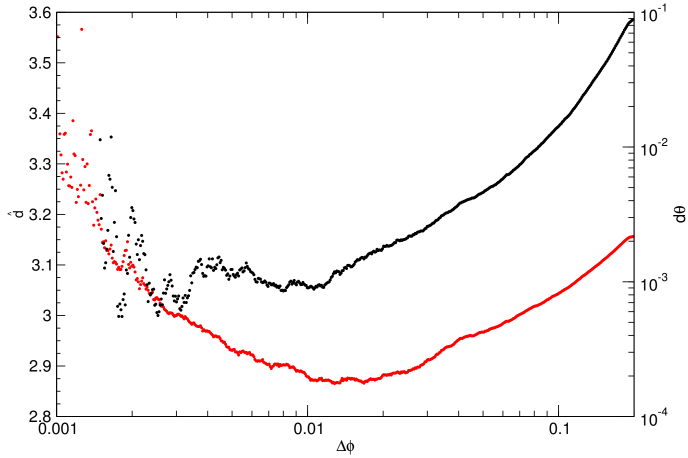

Fig. 13. For a non-saturated packing ($\phi = 0.996$), in black is the estimated value $\hat{d}$ and in red the relative value of error dθ. If the fitting is performed for a $\Delta\phi$ at the end of the plateau of $\hat{d}$, the error is almost minimized.

4.4. Available Surface Function

The kinetics of packing growth at low coverage can be studied in terms of the Available Surface Function (ASF), which is equal to the mean probability of successful deposition using the RSA protocol, for a packing of a given packing fraction

$$\mathrm{ASF}\left(\frac{n}{L^2}\right) = \left\langle \frac{1}{i_n} \right\rangle = \lim_{m\to\infty} \frac{\sum_{k=1}^{m} \frac{1}{i_n}}{m}\,, \tag{4.5}$$

where i_n are the number of iterations required to deposit the n^{th} particle and average is taken over a set of m independent random packings. This implies that ASF is equal to 1 for empty packing and lowers down to 0 at saturation. For loose packings, ASF is typically approximated by a few first terms in the series expansion

$$\mathrm{ASF}(\theta) = 1 - C_1\theta + C_2\theta^2\,. \tag{4.6}$$

Parameters C_1 and C_2 are closely related to the coefficients of virial expansion [31] and, thus, can be used to determine properties of monolayers at equilibrium [32]. Parameter C_1 describes the mean area blocked by a single rectangle, while C_2 corresponds to the mean cross section of these areas for two neighbouring shapes.

Nevertheless, this is not a good fitting for this RSA, especially for low values of α. A much better one is

$$\mathrm{ASF}(\theta) = 1 - C_1\theta + C_n\theta^n\,. \tag{4.7}$$

If we perform the fitting, according to (4.6) and (4.7), respectively, in the range $[0, \theta_{\max}]$, and we plot the coefficients as a function of $\theta_{\max}$ (see Fig. 14), we see that with (4.7), the coefficients C_1 and C_n are almost constant on a

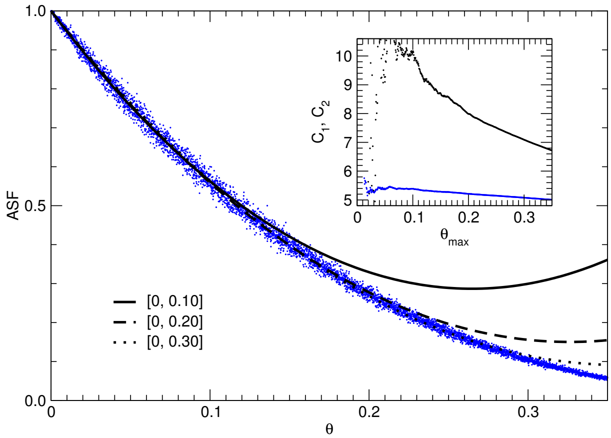

(a)

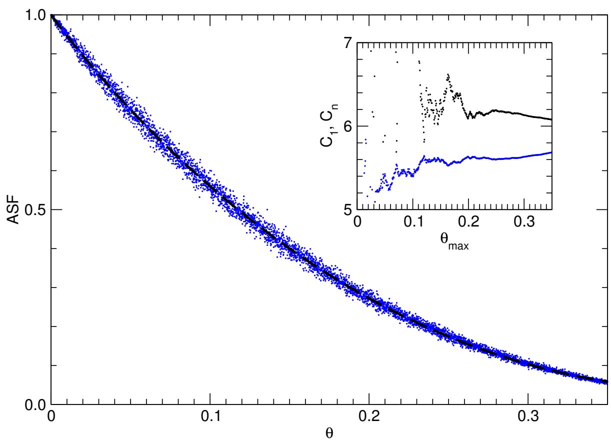

(b)

Fig. 14. In (a), fitting according to (4.6) was performed for $\alpha = 0$ in ranges $[0, \theta_{\max}]$, with $\theta_{\max}$ equal 0.10, 0.20 and 0.30, respectively. This fitting is not satisfactory, since coefficients C_1 (blue) and C_2 (black) are not constant, if $\theta_{\max}$ is changed (see the inset plot). Instead, in (b), there is a plateau for C_1 (blue) and C_n (black): the fitting performed on $[0, 0.20]$ according to (4.7) (dashed line) is good for the whole range $[0, 0.30]$.

wide range of $\theta_{\max}$, while with (4.6), the coefficients (especially C_2) change a lot, depending on which range the fitting has been performed on. Figure 15 also shows that the fitting error with (4.7) is much lower than with (4.6).

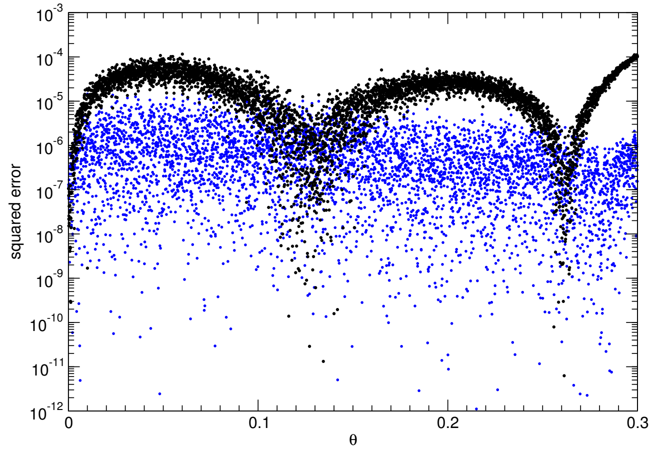

Fig. 15. Squared difference between fittings and ASF, according to (4.6) (black points) and (4.7) (blue points): the latter is much better, as the fitting error is lower and almost constant over the whole range.

The fitting according to (4.7) holds for $\alpha \in (-0.5, +\infty)$, and the coefficients are shown in Fig. 16. For $\alpha \to \infty$, the coefficients converge to the values for squares, as for high αs the probability of choosing 1 as the random aspect ratio goes to 1 (at least, until the saturation of squares, which happens at values of $\theta \approx 0.562$, before the interactions between rectangles start to act and the packing cannot be considered loose anymore).

For squares, the estimated coefficients are, respectively, $C_1 = 3.987 \pm 0.012$, $C_n = 4.26 \pm 0.14$, and $n = 2.085 \pm 0.030$: C_1 is in agreement with the theoretical value, 4.

For $\alpha = 0$, $C_1 = 5.599 \pm 0.022$, $C_n = 6.248 \pm 0.039$, and $n = 1.720 \pm 0.010$: C_1 is in agreement with the theoretical value, 5.555 [15].

On the other hand, for $\alpha \to -1/2$, the two coefficients C_1 and C_n diverge due to the appearance of highly anisotropic shapes, and below that value, up to now, no satisfactory fitting of ASF has been found.

4.5. Two-point correlation function

The two-point correlation function describes the probability of finding two shapes at a given distance r and is defined as

$$g_2(r) = \lim_{\mathrm{d}r \to 0} \frac{N(r, r + \mathrm{d}r)}{2\pi r \theta_{\mathrm{sat}} \mathrm{d}r}\,, \tag{4.8}$$

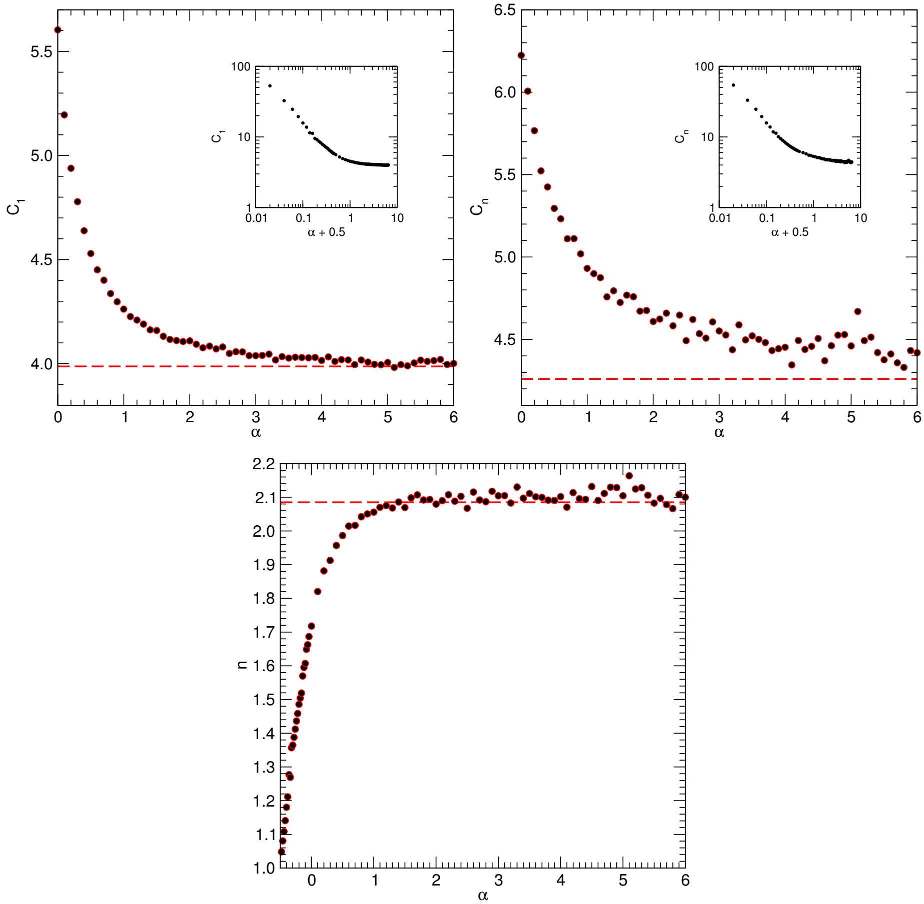

Fig. 16. The coefficients C_1, C_n, and n according to (4.7) as a function of α (the dashed line is the value in the limit of $\alpha \to \infty$).

where $N(r, r + \mathrm{d}r)$ is the mean number of particles with the center at a distance between r and $r + \mathrm{d}r$ from the center of a given particle. The packing fraction θ_{sat} is a normalization factor in order to have $g_2(r \to \infty) = 1$. The function is shown in Fig. 17 and $g_2(r)$ has no logarithmic divergence at contact [22, 33]: in fact, due to the variable shape of the rectangles, theoretically there is no minimal distance between neighbouring shapes centers[5].

[5] In practice, rectangles cannot be too thin, as their longer side cannot be higher than the side of the packing L, but this limit is very small and practically unnoticeable.

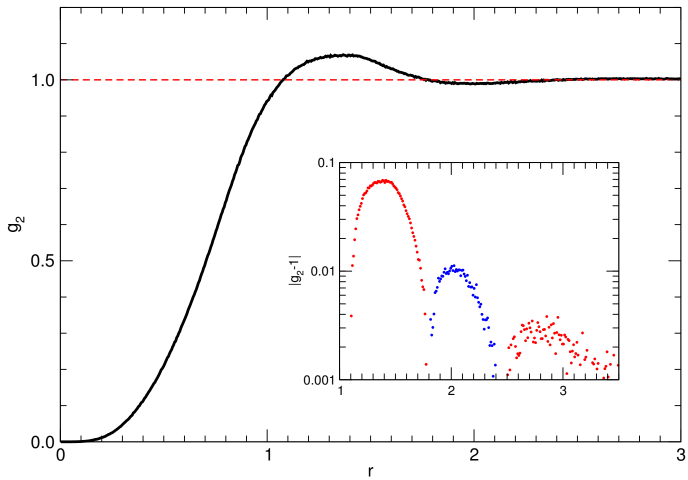

Fig. 17. The density autocorrelation function for rectangles in the RSA packing. In the inset plot, its difference to 1 (in red where positive and in blue where negative): maximum is found for $r \approx \sqrt{2}$, minimum for $r \approx 2$.

4.6. Structure factor

The structure factor is calculated as follows [2]:

$$S(\boldsymbol{k}) = \frac{\left\langle \left|\tilde{\rho}(\boldsymbol{k})^2\right| \right\rangle}{N}, \tag{4.9}$$

where N is the number of rectangles in the periodic square of side length L, the collective density $\tilde{\rho}$ is

$$\tilde{\rho}(\boldsymbol{k}) = \sum_{j=1}^{N} \exp\left(i\boldsymbol{k} \cdot \boldsymbol{r}_j\right) \tag{4.10}$$

and the wave vector $\boldsymbol{k}$ is

$$\boldsymbol{k} = \left(\frac{2\pi n_x}{N}, \frac{2\pi n_y}{N}\right), \tag{4.11}$$

where n_x and n_y are integers.

A packing is hyperuniform if the Structure Factor is vanishing in the limit of wavenumber going to zero [34]. If not, we define

$$S_0 \equiv \lim_{k \to 0} S(k) \tag{4.12}$$

that quantifies how much the packing is distant from being hyperuniform. For this reason, we fit the Structure Factor in the form of

$$S(k) = S_0 + S_2k^2 + S_4k^4 \tag{4.13}$$

for small values of k. The estimated value of S_0 is 0.04055 ± 0.00060 (see Fig. 18), which reveals to be smaller than the value of disks (0.05869 ± 0.00004) [2].

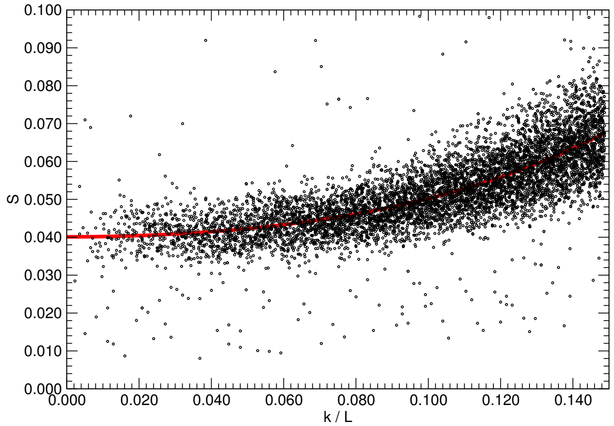

(a)

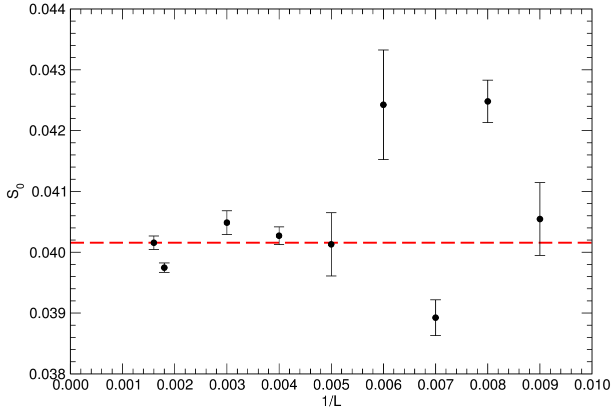

(b)

Fig. 18. (a) The Structure Factor as a function of k/L, obtained as an average of 100 independent packings of size $L = 625$. (b) The estimated value of S_0, performed fitting S according to Eq. (4.13) for $k/L \in [0, 0.15]$, as a function of the inverse of packing size L, with bars denoting the Standard Deviation. The red dashed line corresponds to $S_0 = 0.04055$.

5. Algorithm performance

As described in Section 3, the algorithm allows to reduce the number of unsuccessful tries of deposition with a consequent significant improvement in its performances. In Fig. 19, the number of actual iterations required to reach a density θ using our algorithm is compared with those needed without any reduction in the area over which perform the deposition.

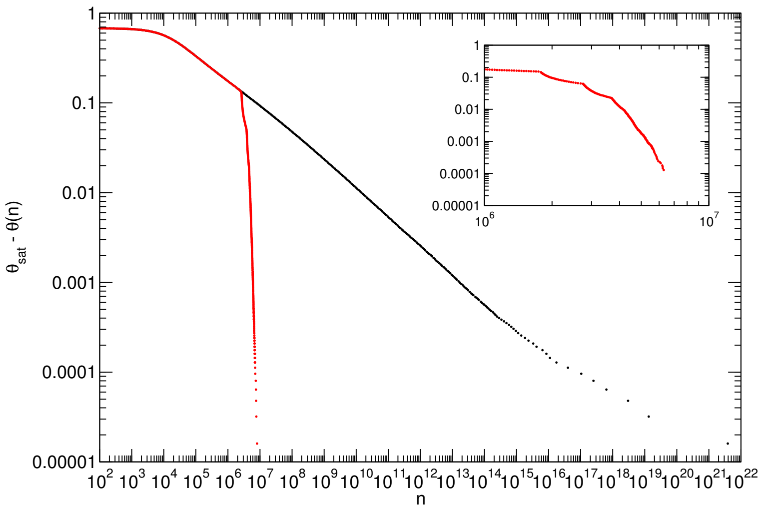

Fig. 19. The actual average number of RSA iterations required to achieve a given value of convergence $\theta_{\mathrm{sat}} - \theta$ is plotted in black, while in red is the number of iterations required using the algorithm. In the inset the same has been plotted for a typical run: the visible cuspids are where the algorithm (1) switches to the search of allowable zones for deposition or (2) reevaluates them (see Ref. [15] for details).

Using this algorithm, we evaluated its performances, function of $S = L^2$ and α, and we found that the complexity is $O(S^2)$ (Fig. 20 (a)), but $O(\mathrm{e}^{\alpha})$ (Fig. 20 (b)) — that is the reason why it is easy to reach very large packings when $\alpha = 0$, but it is too hard to go beyond small values of α.

6. Summary

Here, we investigated the statistical distribution of the density at saturation of RSA of rectangles with random aspect ratio and the performance of the algorithm used in the simulations. We also revisited the analysis of the Available Surface Function and Feder's law, which could be useful also for evaluation of the saturation density using not fully saturated packings.

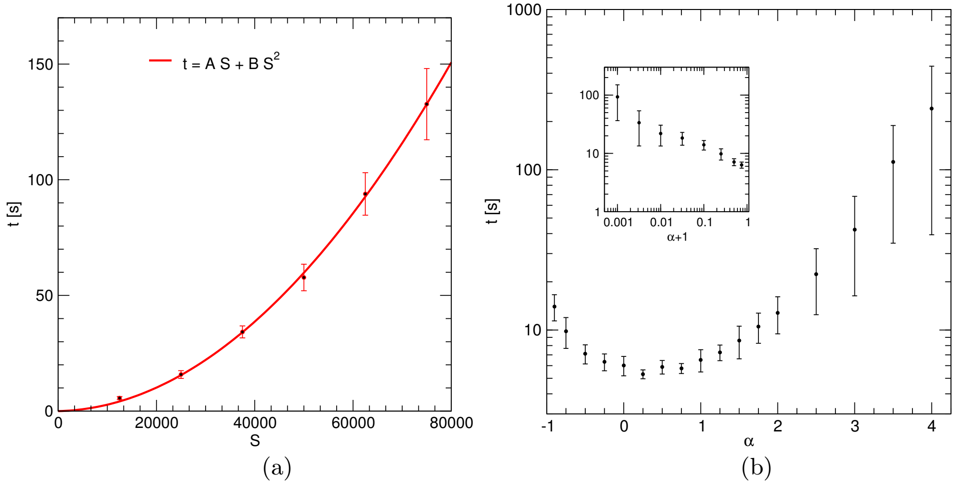

Fig. 20. The average time required to reach saturation (using an Intel® Core™ i7 CPU @ 3.80 GHz) as a function of (a) packing size for $\alpha = 0$ and as a function of (b) α with $L = 125$ (the inset shows the behaviour near $\alpha = -1$) with bars denoting the Standard Deviation.

The Author wants to thank M. Cieśla for his comments and support.

REFERENCES

[1] J. Feder, «Random sequential adsorption», *J. Theor. Biol.* **87**, 237 (1980).

[2] G. Zhang, S. Torquato, «Precise algorithm to generate random sequential addition of hard hyperspheres at saturation», *Phys. Rev. E* **88**, 053312 (2013).

[3] B.J. Brosilow, R.M. Ziff, R.D. Vigil, «Random sequential adsorption of parallel squares», *Phys. Rev. A* **43**, 631 (1991).

[4] G. Zhang, «Precise algorithm to generate random sequential adsorption of hard polygons at saturation», *Phys. Rev. E* **97**, 043311 (2018).

[5] K. Haiduk, P. Kubala, M. Cieśla, «Saturated packings of convex anisotropic objects under random sequential adsorption protocol», *Phys. Rev. E* **98**, 063309 (2018).

[6] M. Cieśla, G. Pajak, R.M. Ziff, «In a search for a shape maximizing packing fraction for two-dimensional random sequential adsorption», *J. Chem. Phys.* **145**, 044708 (2016).

[7] N.I. Lebovka, Y.Y. Tarasevich, «Two-Dimensional Systems of Elongated Particles: From Diluted to Dense», in: Y. Holovatch (Ed.) «Order, Disorder and Criticality», *World Scientific Publishing*, 2020, pp. 153–200.

[8] M. Cieśla, J. Barbasz, «Random packing of regular polygons and star polygons on a flat two-dimensional surface», *Phys. Rev. E* **90**, 022402 (2014).

[9] M. Cieśla, P. Kubala, K. Kozubek, «Algorithms to generate saturated random sequential adsorption packings built of rounded polygons», *Phys. Rev. E* **103**, 063308 (2021).

[10] A.V. Subashiev, S. Luryi, «Fluctuations of the partial filling factors in competitive random sequential adsorption from binary mixtures», *Phys. Rev. E* **76**, 011128 (2007).

[11] M.K. Hassan, J. Schmidt, B. Blasius, J. Kurths, «Jamming coverage in competitive random sequential adsorption of a binary mixture», *Phys. Rev. E* **65**, 045103(R) (2002).

[12] Z. Adamczyk, B. Siwek, M. Zembala, P. Weroński, «Influence of Polydispersity on Random Sequential Adsorption of Spherical Particles», *J. Colloid Interface Sci.* **185**, 236 (1997).

[13] N.V. Brilliantov, Y. A. Andrienko, P.L. Krapivsky, J. Kurths, «Fractal Formation and Ordering in Random Sequential Adsorption», *Phys. Rev. Lett.* **76**, 4058 (1996).

[14] N.V. Brilliantov, Y.A. Andrienko, P.L. Krapivsky, J. Kurths, «Polydisperse adsorption: Pattern formation kinetics, fractal properties, and transition to order», *Phys. Rev. E* **58**, 3530 (1998).

[15] L. Petrone, M. Cieśla, «Random sequential adsorption of oriented rectangles with random aspect ratio», *Phys. Rev. E* **104**, 034903 (2021).

[16] M. Cieśla, A. Nowak, «Managing numerical errors in random sequential adsorption», *Surface Sci.* **651**, 182 (2016).

[17] J.W. Evans, «Random and cooperative sequential adsorption», *Rev. Mod. Phys.* **65**, 1281 (1993).

[18] M. Cieśla, R.M. Ziff, «Boundary conditions in random sequential adsorption», *J. Stat. Mech. Theor. Exp.* **2018**, 043302 (2018).

[19] J.-S. Wang, «A Fast Algorithm for Random Sequential Adsorption of Discs», *Int. J. Mod. Phys. C* **05**, 707 (1994).

[20] W. Kasperek, P. Kubala, M. Cieśla, «Random sequential adsorption of unoriented rectangles at saturation», *Phys. Rev. E* **98**, 063310 (2018).

[21] K. Kozubek, P. Kubala, M. Cieśla, A. Baule, «Exploring 2D shape space: the hunt for the densest RSA packings», Presented at the XXXIV Marian Smoluchowski Symposium on Statistical Physics, 27–29 September, 2021.

[22] R.H. Swendsen, «Dynamics of random sequential adsorption», *Phys. Rev. A* **24**, 504 (1981).

[23] S. Torquato, O.U. Uche, F.H. Stillinger, «Random sequential addition of hard spheres in high Euclidean dimensions», *Phys. Rev. E* **74**, 061308 (2006).

[24] M. Cieśla, J. Barbasz, «Random sequential adsorption on fractals», *J. Chem. Phys.* **137**, 044706 (2012).

[25] M. Cieśla, J. Barbasz, «Random packing of spheres in Menger sponge», *J. Chem. Phys.* **138**, 214704 (2013).

[26] P. Viot, G. Tarjus, «Random Sequential Addition of Unoriented Squares: Breakdown of Swendsen's Conjecture», *Eur. Phys. Lett.* **13**, 295 (1990).

[27] P. Viot, G. Tarjus, S.M. Ricci, J. Talbot, «Random sequential adsorption of anisotropic particles. I. Jamming limit and asymptotic behavior», *J. Chem. Phys.* **97**, 5212 (1992).

[28] E.L. Hinrichsen, J. Feder, T. Jøssang, «Geometry of random sequential adsorption», *J. Stat. Phys.* **44**, 793 (1986).

[29] M. Cieśla, «Continuum random sequential adsorption of polymer on a flat and homogeneous surface», *Phys. Rev. E* **87**, 052401 (2013).

[30] M. Cieśla, «Scaling Properties of the Number of Random Sequential Adsorption Iterations Needed to Generate Saturated Random Packing», *J. Stat. Phys.* **166**, 39 (2017).

[31] S.M. Ricci, J. Talbot, G. Tarjus, P. Viot, «Random sequential adsorption of anisotropic particles. II. Low coverage kinetics», *J. Chem. Phys.* **97**, 5219 (1992).

[32] Z. Adamczyk, «Modeling adsorption of colloids and proteins», *Cur. Opin. Col. Interface Sci.* **17**, 173 (2012).

[33] Y. Pomeau, «Some asymptotic estimates in the random parking problem», *J. Phys. A* **13**, L193 (1980).

[34] S. Torquato, F.H. Stillinger, «Local density fluctuations, hyperuniformity, and order metrics», *Phys. Rev. E* **68**, 041113 (2003).